RSC Advances

PAPER

View Article Online
View Journal | View Issue

Cite this: *RSC Adv.*, 2018, **8**, 39983

A selective detection approach for copper(II) ions using a hydrazone-based colorimetric sensor: spectroscopic and DFT study†

Ismail Abdulazeez, Chanbasha Basheer* and Abdulaziz A. Al-Saadi*

The development of an efficient and miniaturized analytical approach to determine trace levels of toxic ions in aqueous fluids presents a current research challenge. Hydrazone-based chemosensors are considered potential candidates due to their high sensitivity and selectivity towards heavy metal ions. Computational techniques can be properly implemented to elucidate possible modes of ligand–metal interaction and provide an in-depth understanding of the chemistry involved. The present study reports the use of 3-hydroxy-5-nitrobenzaldehyde-4-hydroxybenzoylhydrazone (3-HNHBH) ligand for highly sensitive, quick and re-usable colorimetric sensing of copper(II) ions in aqueous media. DFT calculations suggest that the complexation of 3-HNHBH with copper(II) ions adopts a seesaw coordination geometry and results in the largest HOMO–LUMO gap and most effective coulombic interaction compared to Zn and Ni counterparts. It demonstrated a high selectivity towards copper ions with a detection limit of 0.34 μg L^{-1}. The ligand was readily regenerated using a 0.5 M HCl solution, indicating its feasibility to be used as a re-usable sensor for the convenient detection of copper ions in aqueous media. The influence of metal interference, pH and solvents on the selectivity and regeneration of the ligand was also investigated.

Received 24th October 2018
Accepted 24th November 2018

DOI: 10.1039/c8ra08807a

rsc.li/rsc-advances

1. Introduction

Copper is an essential element that is required in the human body with a delicate balance between deficiency, which could result in ailments such as anemia, and excess, which could cause different types of diseases, such as hypoglycemia and dyslexia.[1] Copper is necessary for the catalytic activity of several physiologically important enzymes.[2] Hereditary copper metabolism disorders and neurodegenerative ailments have been associated with dysfunctional copper-binding proteins and the disruption of cellular homeostasis.[3–5] The common use of copper domestically and industrially has resulted in a widespread exposure and pollution that warrant the development of a means to monitor its level in the environment, water and food.[1,6,7] Conventional techniques for the detection of copper and other heavy metal ions include the use of fluorescent probes,[8] atomic absorption spectrometry,[9,10] inductively coupled plasma-mass spectrometry[11] and electrochemical assays.[12–14] While these analytical methods show an excellent sensitivity, accuracy and selectivity, they lack the convenience in implementation, require specialized instrumentations and need tedious sample pre-treatment before the course of analysis. Hence, recently attentions have been turned to the colorimetry-based detection approach to test for the presence of toxic metal ion traces in aqueous media.[15,16] Such an approach is considered less-labor intensive compared to conventional techniques, offers high sensitivity and selectivity, in addition to cost effectiveness towards the detection of metal ions. One main advantage of colorimetric detections is that it is less capital-intensive and hence exhibits the potential to be developed into simple test kits for on-site and regular inspections.[17]

Several studies have been reported on the colorimetric detection of copper ions in various media. Jo *et al.* reported the synthesis of a multifunctional chemosensor for the detection of cyanide and copper ions.[18] Moreover, a naphthol-based chemosensor for sequential detection of copper and cyanide ions has been reported by Park *et al.*[19] Other functional materials already reported[20–31] for the detection and removal of toxic metal ions at optimum conditions include, hydroxynaphthalene-based,[20,21] quinazoline-based,[22] silica-based,[23,24] hydrazine-based,[25,26] salicylidene-based[27–30] and aroylhydrazone-based[31] compounds. One important conclusion drawn out of these studies was that aroylhydrazone-based sensors could be promising candidates due to the ease of synthesis, fast-response, reusability, and tunable electronic and steric properties along with their chelating ability.[32,33] In the present study, the synthesis of 3-hydroxy-5-nitrobenzaldehyde-4-hydroxybenzoylhydrazone (3-HNHBH), which is a structural isomer of 2-HNHBH,[34] has been reported, and its colorimetric sensing ability towards a number of metal ions, including zinc(II), nickel(II) and copper(II), has been

Department of Chemistry, King Fahd University of Petroleum and Minerals, Dhahran 31261, Saudi Arabia. E-mail: cbasheer@kfupm.edu.sa; asaadi@kfupm.edu.sa

† Electronic supplementary information (ESI) available. See DOI: 10.1039/c8ra08807a

evaluated. Structural parameters, atomic charges and its complexation with these metal ions were predicted using quantum-chemical techniques. Comparison of experimental and computational results provided a better understanding of the underlining chemistry behind the possibly formed complexes.

2. Experimental

All solvents and reagents used were of HPLC grade and used without further purifications. Metal precursors used included nickel(II) acetate, copper(II) acetate, magnesium acetate, calcium acetate, palladium(II) acetate and zinc(II) acetate. Synthesis of 3-hydroxy-5-nitrobenzaldehyde-4-hydroxybenzoylhydrazone (3-HNHBH) ligand was conducted following an already reported procedure[35,36] and then tested with precursors of nickel(II), copper(II), magnesium(II), calcium(II), palladium(II) and zinc(II) ions. Spectroscopic ^{1}H NMR and EDX were used to check the chemical conformation and purity of the ligand before and after complexation with the metal ions, whereas UV-Vis spectroscopy was used to investigate the nature of complexation between the metal ions and the ligand. The UV-visible spectra were recorded on a Shimadzu UV-1601PC spectrophotometer with quartz cells of a 1 cm path length. The ^{1}H nuclear magnetic resonance (NMR) spectra were obtained on a Bruker AV-500 spectrometer in dimethyl sulfoxide (DMSO-d_6) using tetramethylsilane (TMS) as an internal standard. All measurements were performed at the room temperature. Scanning electron microscope (SEM) equipped with energy-dispersive X-ray spectroscope, EDX (Genesis-2120 Emcrafts, Korea Republic) was used to check purity of the ligand and the ligand–metal complexes.

The solutions of 3-HNHBH ligand with tetrahydrofuran (2×10^{-4} M) and acetonitrile (2×10^{-3} M) were prepared and kept under sonication for 10 min. Thereafter, 10 μL of each metal precursor solution was added to 1 mL of a 3-HNHBH ligand solution in a clean glass vial. The resulting mixture was shaken, and changes in color were observed. Another 10 μL quantity of the metal precursor solution was added, and the process carried out again. A similar experiment was conducted with the metal precursors dissolved in THF. For the spectroscopic characterization, 2.5 mL THF was added to 0.5 mL solution of 3-HNHBH ligand in THF (2×10^{-4} M) in a quartz cell, and UV measurements were carried out. Metal precursor solutions in THF were added to the ligand solution in 10 μL aliquots in a quartz cell and the spectra were taken after each addition. For ^{1}H NMR measurements, ligand and metal precursor solutions were prepared in DMSO-d_6 (2×10^{-3} M) in a 1 : 1 ratio. The ligand–metal complex was made by mixing equivolume solutions of the ligand and metal precursors, while the ligand was being analyzed directly.

2.1 Computation

Full geometry optimization and vibrational frequency calculations of the free 3-HNHBH ligand and its metal complexes were carried out using the hybrid B3LYP density functional theory (DFT) approach and the 6-311+G(d) basis set.[37,38] Geometry optimizations of the ligand and complexes formed were carried out to the minima without imposing any constrains on the potential energy surfaces. Relative stabilities of the various forms of the ligand and the total energies of the natural bonding orbitals were obtained. The evaluated binding energies of the ligand and metal ions were obtained following the equation:

$$\text{Binding energy (BE)} = E_{\text{comp}} - (E_{\text{M}}{}^{2+} + 2 \times E_{\text{lig}}) \quad (1)$$

where E_{comp} is the complex's total energy, $E_{\text{M}}{}^{2+}$ and E_{lig} are the energies of the free metal ion and the free ligand, respectively. All calculations were conducted on GAUSSIAN 09 package.[39]

3 Results and discussion

3.1 Ligand and ligand–metal complexes characterization

The selectivity of 3-HNHBH ligand towards a set of various metal ions including Mg(II), Ca(II), Ni(II), Cu(II), Zn(II) and Pd(II) was investigated.[30,40–45] It was observed that only the copper ion solution produced an intensive color change, while the rest of metal ion solutions showed a very mild alteration (Fig. 1) or almost no change in color (Fig. S1†). Hence, the combination of the ligand with copper ions was further investigated by spectroscopic and theoretical means. The 3-HNHBH ligand, like its 2-HNHBH analog reported in a previous study,[34] exhibits two tautomeric keto and enol forms (Fig. 2a). Hydrazonic ligands have been reported to exist as the keto form in the free state, while bind to metal ions in the enol tautomeric form (Fig. 2b).[46,47] From the ^{1}H NMR spectrum of the pure ligand shown in Fig. 3, three distinct resonance peaks are observed at 11.86, 11.17 and 10.18 ppm chemical shifts which can be attributed to the phenolic and amide protons, respectively, indicating that the ligand is keto-tautomeric in a non-coordinated state. Upon complexation with the copper ion, however, a highly deshielded resonance peak at 12.64 ppm which is due to the enolic proton can be observed. This peak appears deshielded since the proton-bearing oxygen atom serves as one of the donor atoms during complexation with the metal ion as shown in Fig. 2b. The presence of the peak associated with the enolic proton confirms the tautomerization of the ligand to the enol form upon complexation (Table S1 and Fig. S2†). The UV-Vis absorption spectra of the ligand in THF showed an absorbance maximum at 347 nm ($\varepsilon_{347} = 4390$ cm^{-1} M^{-1}) due to a symmetry-allowed $\pi \rightarrow \pi^*$ transition rather than a symmetry-forbidden $n \rightarrow \pi^*$ transition. The presence of a single peak suggests the presence of an extended conjugation chain rather than two smaller resonance systems. In addition, two isosbestic points were observed at 315 and 383 nm in the colorimetric titration of the ligand with $Cu(OAc)_2$ (Fig. 4) implying that there are only two absorbing species in the mixture (the free ligand and the ligand–metal complex). The purity and elemental distribution of the ligand and ligand–metal complex were checked by EDX analysis and EDX mapping

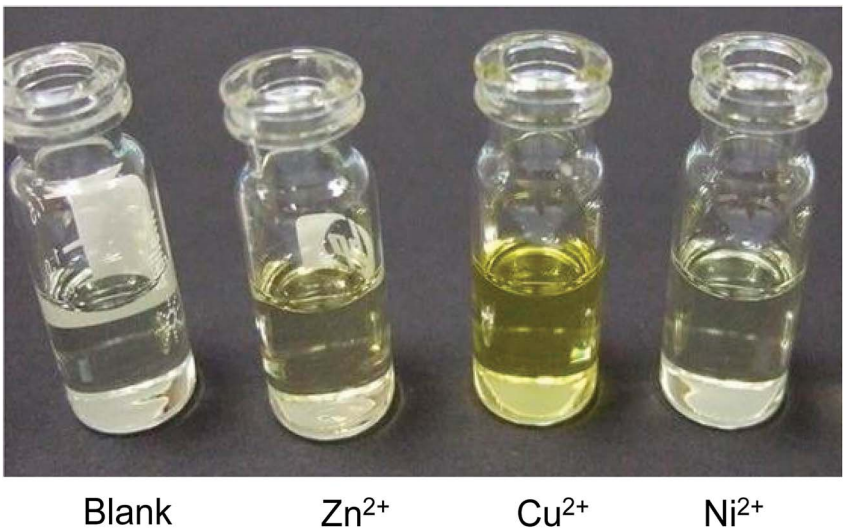

Fig. 1 Color changes observed on addition of 3-HNHBH ligand to $Zn(OAc)_2$, $Cu(OAc)_2$ and $Ni(acac)_2$ solutions. The most intense color change was observed in the case of copper(II) solution.

(Fig. S3 and S4†), and the results confirmed the presence of copper ions in the complex.

DFT method was carried out to further investigate the conformational properties and stabilities of the tautomeric forms of 3-HNHBH before and after complexation. Although the tautomeric forms of the ligand seem to exhibit comparable stabilities, the enol form (enol-b) which is assumed prior to complexation with the metal ion was predicted from DFT calculations to be around 13 kcal mol^{-1} less stable with respect to the most stable keto configuration, as depicted in Fig. 5a. The transition states involving proton transfer from the hydrazonic nitrogen to the carbonyl oxygen to form enol-a lies significantly high (about 70 kcal mol^{-1}) on the potential energy scan. The relative stability suggests that keto to enol-a tautomerization is more likely to take place through an inter- rather than intra-molecular proton-transfer pathway. To facilitate the complexation of 3-HNHBH with the metal ion (Fig. S5†), the calculated TS2 corresponding to the conformational interchange from enol-a to enol-b is predicted to be located at a moderate height of 11 kcal mol^{-1}. The energy profile depicted in Fig. 5a is in

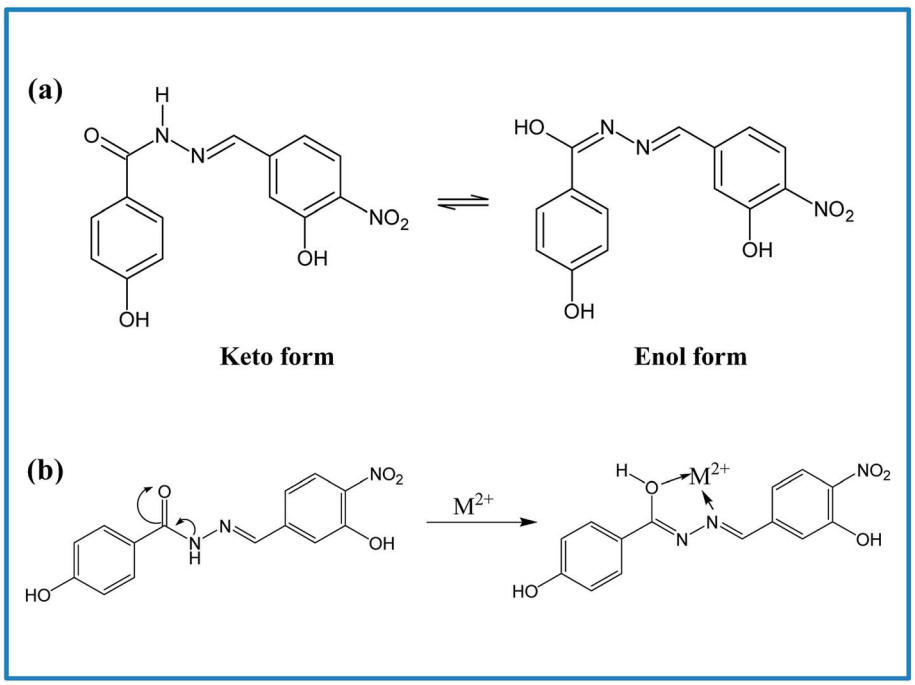

Fig. 2 (a) Keto–enol tautomerization of 3-HNHBH ligand, and (b) the proposed complexation mode of 3-HNHBH ligand with the metal ion center.

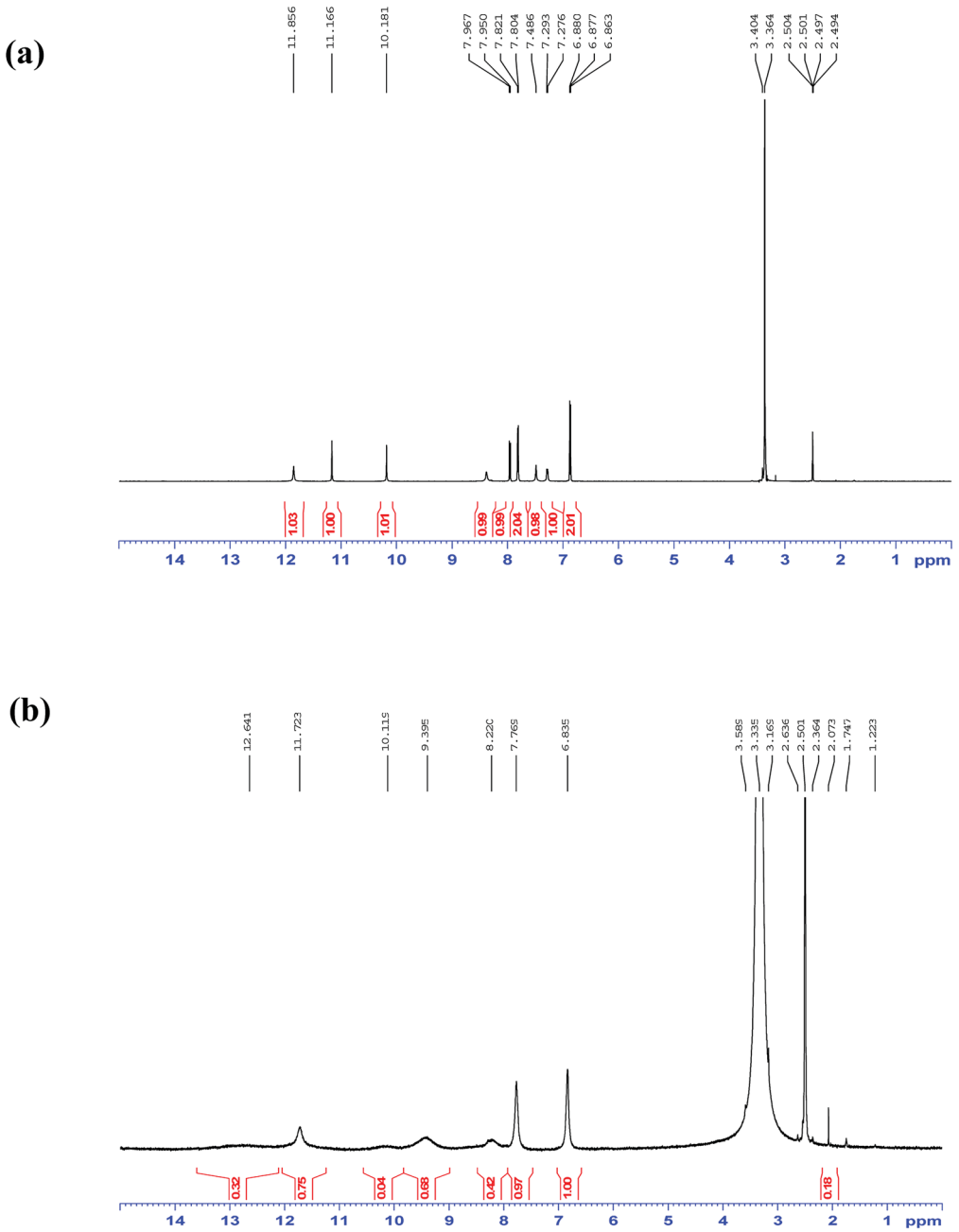

Fig. 3 ^{1}H NMR spectra in DMSO-d_6 of 3-HNHBH ligand (a) before and (b) after complexation with Cu(II) ions.

agreement with the spectroscopic observations and the previous literature reports on the structural and conformational nature of hydrazone-based ligands.[46,47] Moreover, stable configurations of M(3-HNHBH)$_2^{2+}$ complexes (M = Cu, Ni or Zn) were successfully optimized at the B3LYP/6-311+G(d) level of theory and shown in Fig. 5b. It can be noticed that Zn and Cu ions are predicted to adopt a seesaw coordination environment with the ligand compared to a square planar configuration for the Ni counterpart. Furthermore, the bond distance of Cu–O (1.884 Å) was predicted to be shorter than those of Zn–O (2.097 Å) and Ni–O (2.237 Å), indicating a more pronounced coulombic interaction in the case of the copper ion complex which further explains the high sensitivity of the ligand towards Cu(II) ions.

3.2 Effect of parameters

Metal interference effect. Interference solutions containing Ni, Zn, and Cu ions were prepared each at a concentration of 2 × 10^{-3} M and used for colorimetric titrations with 3-HBHBH ligand. When treated with a solution of Ni(II) ions, a solution of Cu(3-HNHBH)$_2^{2+}$ showed no change in color. However, when the Zn(II) solution was added, a slight color change was observed. An inspection of the UV-Vis spectrum of the ligand in the presence of the interference solutions (Fig. 6) showed that the absorption band around 350 nm was gradually decreasing. When the solution was spiked with Cu(OAc)$_2$ in THF, however, it showed a quick response to copper implying the selectivity of

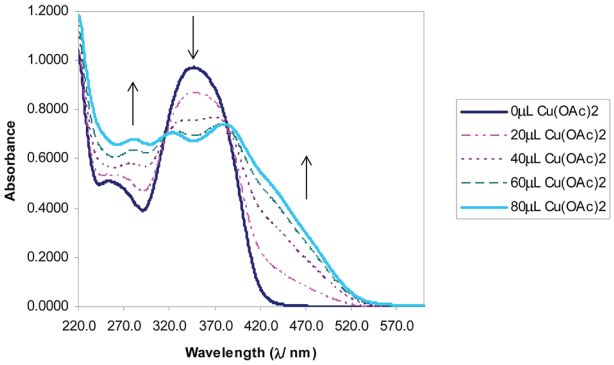

Fig. 4 Absorbance *vs.* wavelength (λ/nm) of ligand/THF with $Cu(OAc)_2$. Some spectra omitted for clarity.

3-HNHBH ligand towards copper(II) ions in the presence of other metal ions. To provide a rational understanding of the interaction nature of 3-HNHBH ligand towards Cu, Ni and Zn metal ions, further investigation at the atomistic level was carried out by calculating metal–ligand binding energies, structural parameters of the optimized complexes and frontier molecular orbitals. Geometrical aspects listed in Table 1 for the three complexes revealed that both Cu and Zn ions tend to adopt a seesaw coordination environment with the nitrogen and oxygen binding sites of the ligand, unlike the Ni ion which undergoes a square planar coordination. The DFT search for the minimum form of the Ni complex showed an appreciable steric repulsion between the two ligand molecules coordinated to the metal ion center, resulting with the least stable binding among the three metal ions. While the seesaw configuration has less experimental evidences in coordinated compounds of zinc and copper,[48–51] it is expected to avail a more stable binding state with the ligand compared to the square planar $Ni(3\text{-HNHBH})_2^{2+}$ metal complex (Table 1). Moreover, while the complexation with Zn(II) ions was predicted to exhibit a relatively higher binding affinity followed by Cu then Ni, careful inspection of the calculated geometrical parameters and the qualitative overview of the structure (Fig. 5b) revealed that Cu ion suits a seesaw coordination environment with 3-HNHBH more conveniently than the Zn analog. The $Cu(3\text{-HNHBH})_2^{2+}$ complex exercises a least deviation from the ideal seesaw arrangement and hence is more feasible of forming a stable complex with the ligand (Table 1). This agrees with the results from preliminary studies presented in Fig. 1 where the ligand exhibited the most intense color change when added to a solution of $Cu(OAc)_2$. Despite having a relatively higher affinity towards Zn(II) which is explained by the competitiveness in interference between these two metals, the ligand was found to be way more selective to Cu(II) ions whose complex with the ligand results with smaller bond distances and closer angles to the ideal seesaw arrangement in comparison with the zinc counterpart. Furthermore, the frontier orbital distribution of 3-HNHBH ligand before and after complexation were computed and shown in Fig. 7. The charge transfer behavior of any two reacting molecules is a function of the spatial orientation of their frontier orbitals and the energy gap maintained as a result of their interaction. The molecular orbital interaction map shows that the ligand's HOMO–LUMO orbitals were fairly delocalized across the molecule, and the electron density located around the hydrazonic nitrogen atoms predicts a more likely binding site present for the metal ion. As expected, upon formation of complex with the metal ions there was a corresponding decrease in energy. The Cu(II) ion complex exhibit the least decrease in energy gap among the three metal ions, which is further indicative of the higher stability of the complex formed with Cu(II) ions relative to the other two metal ions. The relative selectivity of 3-HNHBH towards Cu(II) compared to other metal ions could be attributed to its size that facilities the less usual seesaw coordination sphere with the least relative tilting as a result of binding to the ligand.

Solvent effects. Effects of polar solvents acetonitrile (ACN) and tetrahydrofuran (THF) on the sensitivity and selectivity of 3-HNHBH towards Cu(II) ions was investigated. Preparation of solutions of metal precursors was carried out in 50% (v/v) THF mixed aqueous solutions. The solution was used to dilute the 3-HNHBH ligand at 25% (w/v), 50% (w/v) and 75% (w/v), and tests were carried out on the ligand and metal precursors in mixed aqueous solutions following similar procedure in the preliminary studies. Selectivity of the ligand towards Cu(II) ions increased as a very intense yellowish solution was formed (Table S2†) upon addition of ACN. UV-Vis spectrum of the ligand–metal complex in acetonitrile is presented in Fig. S6.† The spectrum appears similar to that of the complex in pure THF (Fig. 4). Notably, the isosbestic points remained at 315 and 383 nm, but the absorption maximas of the complex shifted slightly from 324 to 330 nm and from 383 to 376 nm. Such observed small hypsochromic shift could be attributed to the addition of ACN which is more polar than THF. The ligand–metal complex in THF/ACN was also observed to absorb more strongly in the region of 420 to 520 nm than the complex in pure THF. This is as a result of the tendency of ACN solvent to stabilize the ligand's non-bonding orbitals *via* hydrogen bonding, and this ultimately increases the amount of energy needed to excite an electron from a non-bonding orbital.

pH effects. Studying the effect of the change in pH of the medium is important as it is expected to impact the sensitivity of 3-HNHBH towards Cu(II) ions. The ligand has been proposed to bind to the metal ion through free electron pairs present on its oxygen and nitrogen atoms. While in the presence of a base it is expected that the nitrogen and oxygen atoms will undergo deprotonation to enhance the binding ability of the ligand to the metal ion, the addition of an acid, on the other hand, tends to protonate the nitrogen and oxygen atoms and thus interferes with the formation of the complex. Such an acid–base protonation–deprotonation process is expected to facilitate–defacilitate the regeneration of the organic ligand. In order to investigate this, aqueous solutions of 2×10^{-4} M 3-HNHBH ligand (0.5 mL) and 2×10^{-3} M metal salts (10 μL) were mixed in glass vials, and 1–10 μL aqueous 0.5 M HCl solution was added followed by aqueous 0.5 M NaOH solution, and *vice versa*. The reason for the choice of NaOH as the investigative base for pH effect was because a solution of the ligand did not produce a color change when NaCl was added. A distinct color change without a noted change in pH was observed when a few drops of

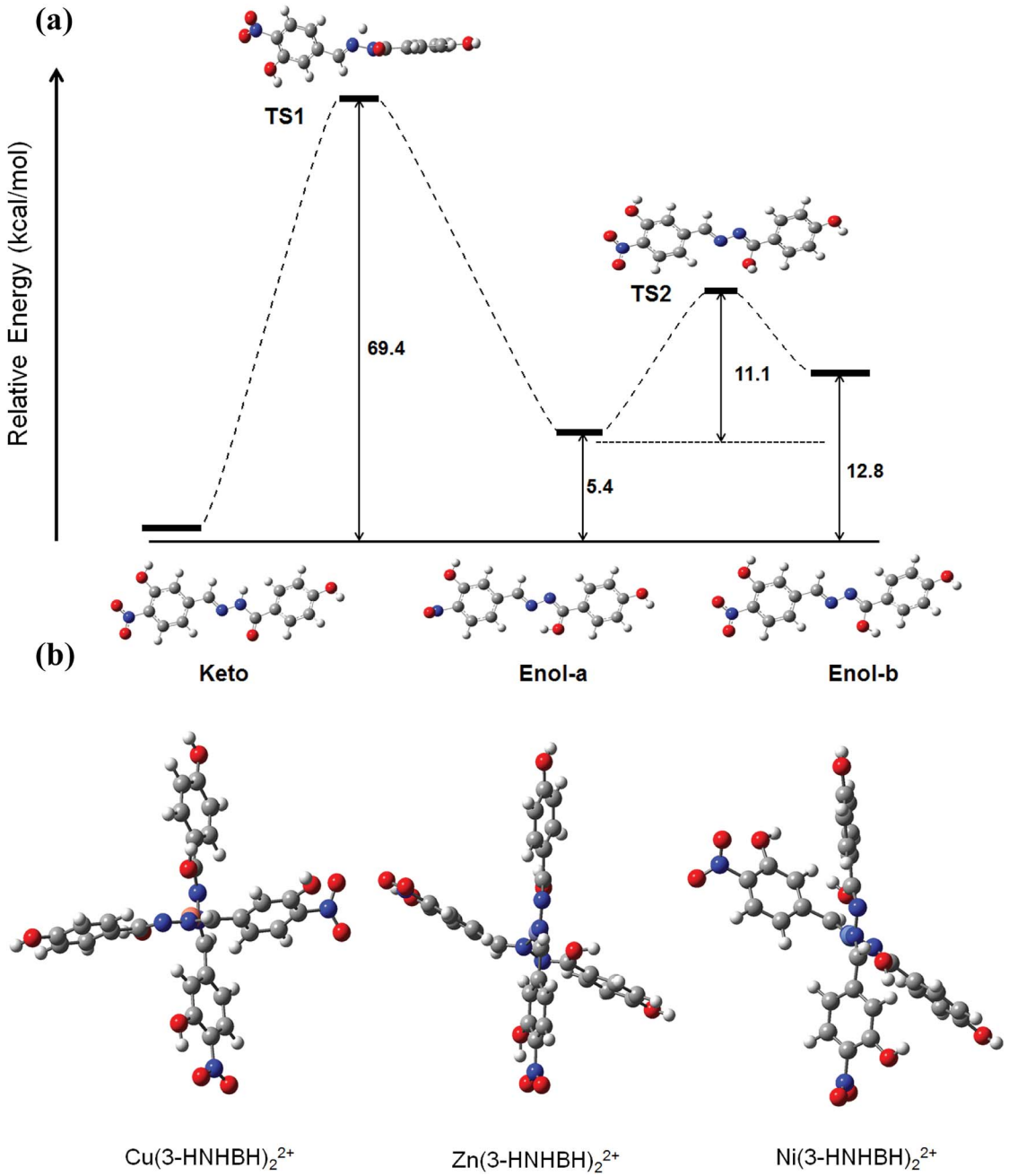

Fig. 5 (a) Suggested step-wise keto–enol tautomerization of 3-HNHBH ligand prior to complexation to the metal ion center, and (b) optimized metal–ligand complexes of 3-HNHBH with Ni(II), Cu(II) and Zn(II) ions, calculated at the B3LYP/6-311+G(d) level of theory.

the acid or base were added to the solution of the ligand. In addition, the color change was observed to be independent of the composition of the mixed aqueous solutions. An addition of the base to a mixed aqueous solution of the ligand and metal precursors increased the selectivity of 3-HNHBH towards Cu(II) as shown in Table 2. Moreover, adding a few drops of a 0.5 M HCl solution to a mixed aqueous solution of the ligand and metal precursors other than Cu(II) ended up with colorless solutions, while a subsequent introduction of Cu(II) ions to the same solution turned it pale-greenish yellow, confirming the preference of 3-HNHBH towards Cu(II) ions.

Further, the selectivity of 3-HNHBH towards copper(II) ions in the presence of EDTA was investigated by preparing 50% THF mixed aqueous solutions of tetrasodium ethylenediaminetetraacetate (Na_4-EDTA) at different concentrations. 50% THF mixed aqueous solutions of 2×10^{-3} M metal salts, $Ni(acac)_2$, $Zn(OAc)_2$, and $Cu(OAc)_2$ were prepared and introduced in 10 μL aliquots to a 0.5 mL Na_4-EDTA solution (2×10^{-4} M) in a glass vial, and color changes were noted. Mixed aqueous solutions of 2×10^{-4} M 3-HNHBH ligand and 10 μL of 2×10^{-3} M metal salts in a glass vial were mixed with 1–10 μL of 2×10^{-2} M and 2×10^{-4} M Na_4-EDTA solutions, respectively. At acidic

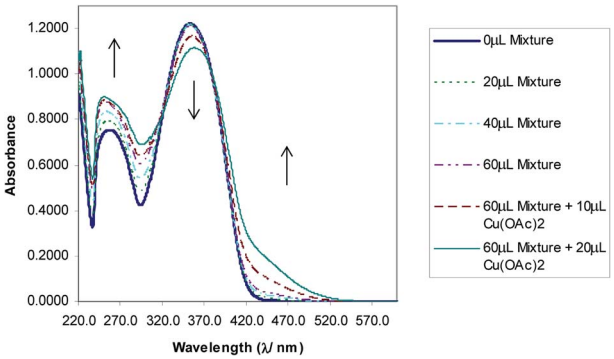

Fig. 6 Absorbance *vs.* wavelength (λ/nm) of ligand/THF with metal interference solutions in THF. Some spectra omitted for clarity.

Table 1 Selected structural parameters and binding energies of metal ion complexes as calculated at the B3LYP/6-311+G(d) level of theory

	$Cu(3\text{-}HNHBH)_2^{2+}$	$Zn\ (3\text{-}HNHBH)_2^{2+}$	$Ni(3\text{-}HNHBH)_2^{2+}$
Bond length (Å)			
M-O	1.884	2.097	2.237
M-N	2.798	2.865	2.899
M-O′	1.889	1.979	1.963
M-N′	2.798	2.873	2.924
Bond angle (deg.)			
N-M-N′	170.11	156.29	177.05
O-M-O′	104.71	109.47	170.56
N-M-O	72.52	77.97	80.74
N′-M-O′	75.95	78.54	80.77
Binding energy (kcal mol^{-1})			
	−196	−226	−169

conditions, a colorless solution was observed, whereas at basic conditions a yellowish color was developed; similar to that which contains no EDTA. At basic condition, the presence of EDTA alone led to the formation of a yellowish color in the presence of 3-HNHBH. This implies that at basic conditions the ligand competes with EDTA in coordinating with Cu(II) ions, with the metal ions having more preference for the ligand. In the acidic condition, however, the ligand is no longer bound to the copper ions which confirm the ligand decomplexation being a means to regenerate the ligand from the complex (Table S3†). It is concluded from all the above observations that the selectivity of 3-HNHBH towards Cu(II) ions could be enhanced in the basic medium, while the acidic medium is shown to facilitate the regeneration of the ligand to its free form.

To determine the sensitivity level of the ligand to varying concentration of copper ions, colorimetric titration was carried out by adding 0.5 mL of the ligand solution in THF (2×10^{-4} M) to 2.5 mL THF in a quartz cell and scanned from 200 to 700 nm. Then, the concentration of the ions was varied by the addition of 10 μL aliquots, and the UV-Vis spectra were recorded. A corresponding linear response was observed (Fig. S7†) with a detection limit (S/N = 3) of 0.34 μg L^{-1}.

The influence of acid or base additions can be further explained in terms of keto–enol tautomerism of 3-HNHBH ligand. Keto–enol tautomerization refers to a chemical equilibrium that exists between the two forms of the molecule; namely the keto form having a carbonyl group and the enol form having a pair of doubly bonded atoms adjacent to a hydroxyl group. Addition of a 0.5 M HCl solution therefore protonates the enolic hydroxyl group releasing the metal ions from the ligand–metal complex, while addition of 0.5 M NaOH solution improves the preference of the ligand for the metal

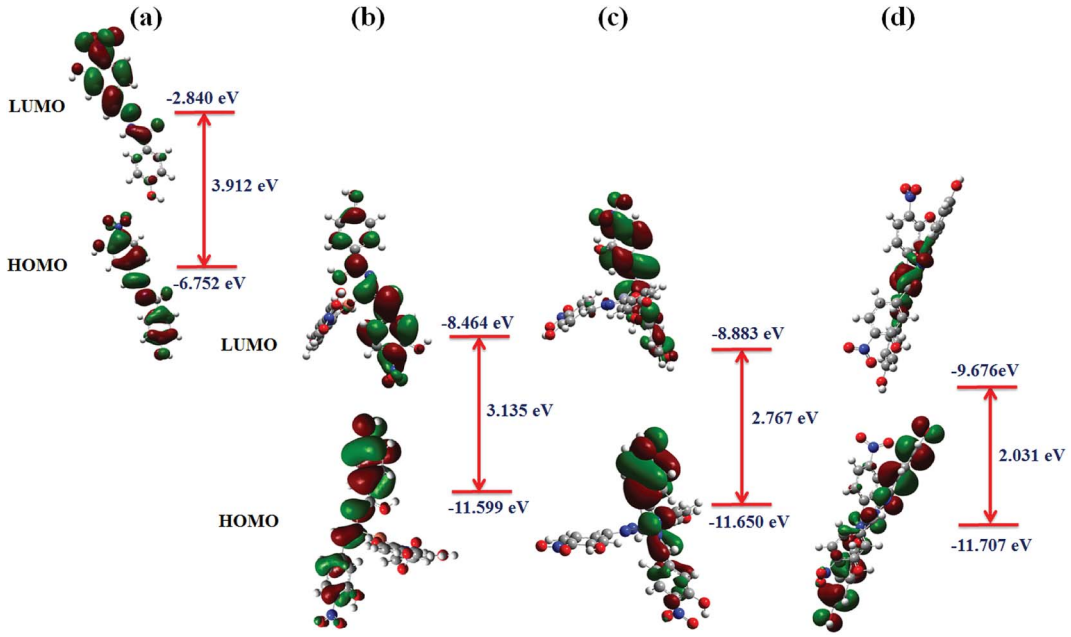

Fig. 7 Calculated frontier molecular orbitals of 3-HNHBH and the corresponding HOMO and LUMO orbital energies (a) before, and after complexation with (b) Cu(II), (c) Zn(II) and (d) Ni(II) metal ions.

Table 2 Description of color changes when aqueous solutions of NaOH and HCl are added to 3-HNHBH solutions of metal salts

Metal salt		$Ni(acac)_2$	$Cu(OAc)_2$	$Zn(OAc)_2$
Initial solution color		Pale green-yellow	Pale green-yellow	Very, very pale green-yellow
Set 1	+1 μL NaOH	Greenish-yellow	Bright-yellow	Greenish-yellow
	+1 μL HCl	Colourless	Pale green-yellow	Colourless
Set 2	+1 μL HCl	Colourless	Colourless	Colourless
	+2 μL NaOH	Greenish-yellow	Pale green-yellow	Greenish-yellow

Table 3 Calculated Mullikan Atomic charges (e^-) on selected atoms of the 3-HNHBH ligand

Atom	Charge
O	−0.697
N	−0.327
O_a	−0.601
O_h	−0.641

ions. To further elucidate the effect of change in pH on the complexation of 3-HNHBH with metal ions, Mulliken atomic charge distribution on the atoms of the ligand were calculated (Fig. S8†). Atomic charges on prominent sites of the ligand where protonation is expected to take place are summarized in Table 3. The atomic charge distribution is normally used to predict chemical reactivities of a given molecule under various pH conditions. It provides useful insights on the electronic features of the molecule, and from this it is possible to predict bonding, anti-bonding or non-bonding features of the molecule.[52] The calculated atomic charges for the 3-HNHBH complex were remarkably negative on the oxygen atoms of the carbonyl group and hydroxyl group *para* to carbonyl (O and O_h) as shown in Table 3. This correlates with experimental results in which the addition of a strong acid even at small quantities results in discoloration of the complex as a result of fast protonation of the hydroxyl and carbonyl oxygen atoms.

4 Conclusion

A hydrazone-based ligand was synthesized and utilized for possible colorimetric sensing of copper(II) ions. The ligand displayed good selectivity and sensitivity towards Cu(II) ions over zinc and nickel analogs with a detection limit of 0.34 μg L^{-1}. Electronic calculations utilizing the DFT approach suggested that the complexation of 3-HNHBH with the metal ions is initiated *via* a keto–enol tautomerization followed by a hydroxyl-group internal rotation to overcome the intramolecular hydrogen bonding. The selectivity of 3-HNHBH ligand towards copper ions improved slightly when a small amount of acetonitrile was added, whereas it could not be ascertained in THF–water mixed aqueous solutions. In addition, treating the Cu(3-HNHBH)$_2^{2+}$ complex in a mixed aqueous solution with EDTA followed by the addition of a few drops a mildly acidic solution could successfully regenerate the original ligand, indicating that the organic-based 3-HNHBH ligand can be considered an attractive choice for the development of a reusable sensor for cupper ions in aqueous media.

Conflicts of interest

The authors declare no competing financial interest.

Acknowledgements

Authors gratefully acknowledge the support of this work by King Fahd University of Petroleum and Minerals (KFUPM).

References

1 N. Aksuner, E. Henden, I. Yilmaz and A. Cukurovali, *Dyes Pigm.*, 2009, **83**, 211–217.
2 D. Strausak, J. F. B. Mercer, H. H. Dieter, W. Stremmel and G. Multhaup, *Brain Res. Bull.*, 2001, **55**, 175–185.
3 D. R. Brown and H. Kozlowski, *Dalton Trans.*, 2004, 1907–1917, DOI: 10.1039/b401985g.
4 D. J. Waggoner, T. B. Bartnikas and J. D. Gitlin, *Neurobiol. Dis.*, 1999, **6**, 221–230.
5 H.-G. Li, Z.-Y. Yang and D.-D. Qin, *Inorg. Chem. Commun.*, 2009, **12**, 494–497.
6 V. K. Gupta, A. K. Jain, G. Maheshwari, H. Lang and Z. Ishtaiwi, *Sens. Actuators, B*, 2006, **117**, 99–106.
7 X. Q. Chen, M. J. Jou, H. Lee, S. Z. Kou, J. Lim, S. W. Nam, S. Park, K. M. Kim and J. Yoon, *Sens. Actuators, B*, 2009, **137**, 597–602.
8 L. Sen, T. Jingqi, W. Lei, Z. Yingwei, Q. Xiaoyun, L. Yonglan, A. M. Abdullah, A.-Y. O. Abdulrahman and S. Xuping, *Adv. Mater.*, 2012, **24**, 2037–2041.
9 S. L. C. Ferreira, M. A. Bezerra, A. S. Santos, W. N. L. dos Santos, C. G. Novaes, O. M. C. de Oliveira, M. L. Oliveira and R. L. Garcia, *TrAC, Trends Anal. Chem.*, 2018, **100**, 1–6.
10 L. Fernández-López, B. Gómez-Nieto, M. J. Gismera, M. T. Sevilla and J. R. Procopio, *Spectrochim. Acta, Part B*, 2018, **147**, 21–27.
11 I. D. la Calle, P. Pérez-Rodríguez, D. Soto-Gómez and J. E. López-Periago, *Microchem. J.*, 2017, **133**, 293–301.
12 L. Tian, J. Qi, K. Qian, O. Oderinde, Q. Liu, C. Yao, W. Song and Y. Wang, *J. Electroanal. Chem.*, 2018, **812**, 1–9.
13 A. Ismail, A. Kawde, O. Muraza, M. A. Sanhoob and A. R. Al-Betar, *Microporous Mesoporous Mater.*, 2016, **225**, 164–173.
14 A. Kawde, A. Ismail, A. R. Al-Betar and O. Muraza, *Microporous Mesoporous Mater.*, 2017, **243**, 1–8.
15 Y. Ping, Z. Chen, Q. Ding, Q. Zheng, Y. Lin and Y. Peng, *Tetrahedron*, 2017, **73**, 594–603.

16 F.-U. Rahman, S.-B. Yu, S. K. Khalil, Y. P. Wu, S. Koppireddi, Z.-T. Li, H. Wang and D.-W. Zhang, *Sens. Actuators, B*, 2018, **263**, 594–604.
17 R. Sheng, P. Wang, Y. Gao, Y. Wu, W. Liu, J. Ma, H. Li and S. Wu, *Org. Lett.*, 2008, **10**, 5015–5018.
18 T. G. Jo, Y. J. Na, J. J. Lee, M. M. Lee, S. Y. Lee and C. Kim, *Sens. Actuators, B*, 2015, **211**, 498–506.
19 G. J. Park, I. H. Hwang, E. J. Song, H. Kim and C. Kim, *Tetrahedron*, 2014, **70**, 2822–2828.
20 S. A. Lee, J. J. Lee, J. W. Shin, K. S. Min and C. Kim, *Dyes Pigm.*, 2015, **116**, 131–138.
21 M. R. Awual, T. Yaita and Y. Okamoto, *Sens. Actuators, B*, 2014, **203**, 71–80.
22 A. Mohammadi and S. Yaghoubi, *Sens. Actuators, B*, 2017, **241**, 1069–1075.
23 M. R. Awual, M. Ismael, T. Yaita, S. A. El-Safty, H. Shiwaku, Y. Okamoto and S. Suzuki, *Chem. Eng. J.*, 2013, **222**, 67–76.
24 M. R. Awual and M. M. Hasan, *Sens. Actuators, B*, 2015, **206**, 692–700.
25 M. R. Awual, T. Yaita, S. A. El-Safty, H. Shiwaku, S. Suzuki and Y. Okamoto, *Chem. Eng. J.*, 2013, **221**, 322–330.
26 M. R. Awual, I. M. M. Rahman, T. Yaita, M. A. Khaleque and M. Ferdows, *Chem. Eng. J.*, 2014, **236**, 100–109.
27 M. R. Awual, *Chem. Eng. J.*, 2015, **266**, 368–375.
28 M. R. Awual, M. M. Hasan, M. A. Khaleque and M. C. Sheikh, *Chem. Eng. J.*, 2016, **288**, 368–376.
29 M. R. Awual, *Chem. Eng. J.*, 2017, **307**, 85–94.
30 M. R. Awual, *J. Ind. Eng. Chem.*, 2014, **20**, 3493–3501.
31 M. Pannipara, A. G. Al-Sehemi, M. Assiri and A. Kalam, *Opt. Mater.*, 2018, **79**, 255–258.
32 S. Naskar, S. Naskar, S. Mondal, P. K. Majhi, M. G. B. Drew and S. K. Chattopadhyay, *Inorg. Chim. Acta*, 2011, **371**, 100–106.
33 A.-M. Stadler and J. Harrowfield, *Inorg. Chim. Acta*, 2009, **362**, 4298–4314.
34 I. Abdulazeez, C. Basheer and A. A. Al-Saadi, *J. Mol. Liq.*, 2018, **264**, 58–65.
35 P. Melnyk, V. Leroux, C. Sergheraert and P. Grellier, *Bioorg. Med. Chem. Lett.*, 2006, **16**, 31–35.
36 A. A. Tameem, A. Salhin, B. Saad, I. A. Rahman, M. I. Saleh, S.-L. Ng and H.-K. Fun, *Acta Crystallogr., Sect. E: Struct. Rep. Online*, 2007, **63**, o57–o58.
37 A. D. Becke, *J. Chem. Phys.*, 1993, **98**, 5648–5652.
38 C. Lee, W. Yang and R. G. Parr, *Phys. Rev. B: Condens. Matter Mater. Phys.*, 1988, **37**, 785–789.
39 M. J. Frisch, G. W. Trucks, H. B. Schlegel, G. E. Scuseria, M. A. Robb, J. R. Cheeseman, G. Scalmani, V. Barone, B. Mennucci, G. A. Petersson, H. Nakatsuji, M. Caricato, X. Li, H. P. Hratchian, A. F. Izmaylov, J. Bloino, G. Zheng, J. L. Sonnenberg, M. Hada, M. Ehara, K. Toyota, R. Fukuda, J. Hasegawa, M. Ishida, T. Nakajima, Y. Honda, O. Kitao, H. Nakai, T. Vreven, J. A. Montgomery, J. E. Peralta, F. Ogliaro, M. Bearpark, J. J. Heyd, E. Brothers, K. N. Kudin, V. N. Staroverov, R. Kobayashi, J. Normand, K. Raghavachari, A. Rendell, J. C. Burant, S. S. Iyengar, J. Tomasi, M. Cossi, N. Rega, J. M. Millam, M. Klene, J. E. Knox, J. B. Cross, V. Bakken, C. Adamo, J. Jaramillo, R. Gomperts, R. E. Stratmann, O. Yazyev, A. J. Austin, R. Cammi, C. Pomelli, J. W. Ochterski, R. L. Martin, K. Morokuma, V. G. Zakrzewski, G. A. Voth, P. Salvador, J. J. Dannenberg, S. Dapprich, A. D. Daniels, O. Farkas, J. B. Foresman, J. V. Ortiz, J. Cioslowski and D. J. Fox, *Gaussian 09, revision b.01*, 2009.
40 M. R. Awual, M. A. Khaleque, Y. Ratna and H. Znad, *J. Ind. Eng. Chem.*, 2015, **21**, 405–413.
41 M. R. Awual, T. Yaita, H. Shiwaku and S. Suzuki, *Chem. Eng. J.*, 2015, **276**, 1–10.
42 M. R. Awual, M. Khraisheh, N. H. Alharthi, M. Luqman, A. Islam, M. Rezaul Karim, M. M. Rahman and M. A. Khaleque, *Chem. Eng. J.*, 2018, **343**, 118–127.
43 M. R. Awual, M. M. Hasan, G. E. Eldesoky, M. A. Khaleque, M. M. Rahman and M. Naushad, *Chem. Eng. J.*, 2016, **290**, 243–251.
44 M. R. Awual and M. M. Hasan, *Sens. Actuators, B*, 2014, **202**, 395–403.
45 M. R. Awual, M. M. Hasan and M. A. Khaleque, *Sens. Actuators, B*, 2015, **209**, 194–202.
46 M. V. Angelusiu, S.-F. Barbuceanu, C. Draghici and G. L. Almajan, *Eur. J. Med. Chem.*, 2010, **45**, 2055–2062.
47 R. Gup and B. Kırkan, *Spectrochim. Acta, Part A*, 2005, **62**, 1188–1195.
48 J. A. Bellow, D. Fang, N. Kovacevic, P. D. Martin, J. Shearer, G. A. Cisneros and S. Groysman, *Chem.–Eur. J.*, 2013, **19**, 12225–12228.
49 S. Fox, R. T. Stibrany, J. A. Potenza, S. Knapp and H. J. Schugar, *Inorg. Chem.*, 2000, **39**, 4950–4961.
50 L. Yang, D. R. Powell and R. P. Houser, *Dalton Trans.*, 2007, 955–964, DOI: 10.1039/b617136b.
51 T. Chu, L. Belding, P. K. Poddutoori, A. van der Est, T. Dudding, I. Korobkov and G. I. Nikonov, *Dalton Trans.*, 2016, **45**, 13440–13448.
52 M.-J. Lee and B.-D. Lee, *Tetrahedron Lett.*, 2010, **51**, 3782–3785.